Estimating the impact of natural and anthropogenic emissions on cloud chemistry: the influence of organic compounds

L. Alfonso, G. B. Raga

Atmos. Chem. Phys. Discuss., 4, 591–634, 2004
www.atmos-chem-phys.org/acpd/4/591/
SRef-ID: 1680-7375/acpd/2004-4-591

Atmospheric Chemistry and Physics Discussions

Estimating the impact of natural and anthropogenic emissions on cloud chemistry: the influence of organic compounds

L. Alfonso and G. B. Raga

Centro de Ciencias de la Atmósfera, UNAM, Mexico City, 04510, Mexico

Received: 21 November 2003 – Accepted: 21 January 2004 – Published: 26 January 2004

Correspondence to: L. Alfonso (lesterson@yahoo.com)

Abstract

In order to estimate the anthropogenic influence of gas and aerosol emissions from the Petroleum Industry in maritime zones with clouds of small vertical extent, a numerical 1D Eulerian cloud-chemical model with detailed microphysics (Alfonso and Raga, 2002) is used to simulate the influence of water soluble organic compounds (WSOC) and organic+inorganic gas emissions on cloud development. Following Mircea et al. (2002), we tested the sensitivity of the cloud and precipitation development in the classical inorganic case (CIC) and the inorganic+organic case (IOC) with respect to CCN compositions. The results indicate an increase in the droplet concentration for the IOC, and a delay in the development of precipitation.

The pH spectral evolution was studied during both the development and precipitation stages. The influence of the diffusion of formic acid and its generation by oxidation of hydrated formaldehyde in the aqueous phase result in a reduction in the pH of precipitation in the range between 0.05 and 0.15 pH units (from 1 to 3%) for the high ambient SO_2 concentration (20 ppb) and between 0.2–0.5 pH units (from 4 to 10%) for the low ambient SO_2 concentration (1 ppb) case.

1. Introduction

It has been known for many years that radically different cloud condensation nuclei (CCN) size distributions and compositions, play a clear role in precipitation development. Even though a large number of efforts have been conducted to address this subject, the role of organic compounds in the microphysical and dynamical structure of clouds remains unclear. Within the present discussion on climate change, the role of organic carbon has gained more attention. A number of attemps to obtain a mass balance of organic carbon (OC) in the aerosols have been carried out, but no available identification of individual compounds has been possible so far (Saxena and Hildemann, 1996).

ACPD
4, 591–634, 2004

Likens et al. (1983) studied the potential role of organic compounds in the chemistry of wet aerosols many years ago. Recently, the contribution of organic aerosols to the mass of cloud condensation nuclei (CCN) has been brought back as an unresolved topic (Novakov and Penner, 1993; Corrigan and Novakov, 1999). They reported that pure organic smoke aerosols from cellulose combustion are efficient CCN without being associated to inorganic salts.

Sources of monocarboxylic acids in the tropospheric gaseous, aerosol and aqueous phase comprise anthropogenic and biogenic emissions and chemical transformations of precursors, while dicarboxylic acids are likely to be found principally in aerosol from primary sources. Various sources of organic acids in the atmosphere were mentioned by Chebbi and Carlier (1996) including: plastic combustions, tobacco smoke, chemical plant transformations, refuse incineration factories, biomass burning, motor vehicle exhausts and aqueous phase reactions in drops (Yao et al., 2002).

Formic, acetic and other lightweight carboxylic acids, formaldehyde and other gas phase derived species were reported by Facchini et al. (1999) to constitute dissolved organic compounds. Löflund et al. (2002) and Hegg et al. (2002) measured concentrations of carboxylic and dicarboxylic acids in continental and maritime cloud water. Low weight dicarboxylic acids are hygroscopic and have recently received much attention because of their potential effects in cloud formation (Cruz and Pandis, 1997).

Facchini (2001) also studied the photochemical formation of formic acid in clouds. The remaining part of the organic carbon was considered insoluble in cloud water and the effects of organic compounds were mainly linked to the formation of organic films on the surface of droplets. Organic films may be common in water droplets and may retard evaporation and condensation. The possible implications for cloud spectral broadening were recently reported by Feingold and Chuang (2002).

Barth et al. (2000) reported results obtained with a three-dimensional, fully-compressible cloud model, that includes organics in both gas and aqueous-phase modules. The aqueous-phase chemistry is computed for cloud water and rain assuming a pH of 4.5, and only bulk microphysics is considered. They reported that H_2O_2 is

ACPD
4, 591–634, 2004

somewhat reduced in the outflow region of the storm by aqueous chemistry, but is substantially reduced when the ice microphysics is included in the simulations and frozen hydrometeors are allowed to capture H_2O_2. Their simulations do not allow them to look at the evolution of pH as the precipitation develops, since they used a fixed value.

In this study we present results from a theoretical 1-D cloud model that includes detailed microphysics and organic and inorganic chemistry. The main two goals of our investigation are:

1. To study the influence of water- soluble organic compounds (WSOC) on CCN activation and droplet concentration.
2. To study the impact of chemical reactions both inorganic and simple organics to attempt to estimate their impact on precipitation acidification.

The role of water soluble organic compounds (WSOC) in the pH spectra of precipitation, is beyond the scope of the study and wasn't included in the analysis.

2. The cloud chemistry model

2.1. Microphysics

The model microphysics follows Alfonso and Raga (2002) (hereafter denoted as AR2002) and includes the following microphysical processes: nucleation of CCN, condensation and evaporation, collision and coalescence, and breakup. The cloud and CCN spectra are discretized using the method described by Berry (1967). For CCN composition, we consider two cases: the classical inorganic case (CIC), assuming that CCN are composed only by inorganic compounds and the inorganic + organic case (IOC), when CCN composition includes inorganic and WSOC, as discussed in more detailed in Sect. 2.3.1.

There are 64 bins for the entire CCN spectrum (from 0.0041 to 5.93 μm), 48 bins for the small droplets (from 0.0041 to 1 μm) and 73 bins for the rest of the spectrum (from

ACPD
4, 591–634, 2004

1 to 4096 μm). The procedures for calculating activation, condensation, coalescence and breakup are described in AR2002.

The additional grid for small droplets (from 0.0041 to 1 μm) was introduced in order to reduce the numerical diffusion by interpolation during activation, since this is an eulerian model, and there is a need to interpolate onto a fixed grid. After CCN activation, there is a possibility of forming droplets smaller than 1 μm, that are interpolated in this grid. By doing this, the artificial increase in droplet concentration at the small end of the spectrum (for droplets larger than 1 μm) observed in some models is avoided. There is no evolution by coalescence and breakup for these small droplets.

2.2. Dynamics

As discussed in AR2002, the model dynamics is based on the one-dimensional framework developed by Asai and Kasahara (1967), where a cylindrical cloud of constant radius develops in an environment at rest. All equations are expressed in terms of cylindrical coordinates and cloud variables are represented by mean values averaged over the horizontal cross section of the cloud.

The dynamic equations are solved for the vertical air velocity, w; radial air velocity, u_a; temperature, T; water vapor mixing ratio, Q_v; for cloud condensation nuclei (CCN) number density in category i, $(f(i))$, with a maximum of 64 categories from 0.0041 to 5.93 μm; for cloud number density function for small droplets in category j, $f_{ds}(j)$, with a maximum of 48 categories from 0.0041 to 1 μm; for cloud number density function for large drops in category j, $f_d(j)$, with a maximum of 73 categories from 1 to 4096 μm; for the mass density functions of particles in small droplets and drops in category j, $(g_{ds}(j), g_d(j))$; for the mass density function of chemical species for small droplets and drops in category j, $(g_{dsC}(j), g_{dC}(j))$; and for the concentration of gases (C_g) in the air.

Dynamic equations for vertical air velocity, w; radial air velocity, u_a; temperature, T; water vapor mixing ratio, Q_v are described in detail in Alfonso et al. (1998) and AR2002.

ACPD
4, 591–634, 2004

We assumed for every variable A (Ogura and Takahashi, 1971) that

$A_a = A_e$ if $u_a < 0$

$A_a = A$ if $u_a > 0$

here A_e denotes environmental parameters, while A_a refers to values at the perimeter of the cloud, and A refers to values inside the cloud. The distribution functions are calculated through the following equations, and a description of each term is given immediately following the equations.

The evolution of the CCN number density, $f(i)$, for every category i (from 0.0041 to 5.98 μm, 64 categories) is calculated as:

$$\frac{\partial f(i)}{\partial t} = -w\frac{\partial f(i)}{\partial z} - 2\frac{\alpha^2}{a}|w|[f(i) - f_e(i)]$$
$$+\frac{2}{a}u_a[f(i) - f_a(i)] + \frac{1}{\rho_a}\frac{\partial}{\partial z}\left(\rho_a K\frac{\partial f(i)}{\partial z}\right) + \left(\frac{\partial f(i)}{\partial t}\right)_{act}, \quad (1)$$

where the term $(\partial/\partial t)_{act}$ corresponds to the activation of CCN. Two distributions are calculated, $f(i)_{CIC}$ and $f(i)_{IOC}$ for the classical inorganic ($(NH_4)_2SO_4$) and the inorganic+organic ($(NH_4)_2SO_4$+WSOC) cases, respectively.

The time evolution of the cloud number density functions for small droplets, $f_{ds}(j)$, for each category, from 0.0041 to 1 μm (48 categories) is calculated according to:

$$\frac{\partial f_{ds}(j)}{\partial t} = -w\frac{\partial f_{ds}(j)}{\partial z} - 2\frac{\alpha^2}{a}|w|[f_{ds}(j) - f_{dse}(j)]$$
$$+\frac{2}{a}u_a[f_{ds}(j) - f_{dsa}(j)] + \frac{1}{\rho_a}\frac{\partial}{\partial z}\left(\rho_a K\frac{\partial f_{ds}(j)}{\partial z}\right)$$
$$+\left(\frac{\partial f_{ds}(j)}{\partial t}\right)_{act} + \left(\frac{\partial f_{ds}(j)}{\partial t}\right)_{CE}. \quad (2)$$

ACPD
4, 591–634, 2004

Now, not only the the activation term is present, but also a term $(\partial/\partial t)_{CE}$ that represents droplet growth by condensation or decrease by evaporation.

The cloud number density distribution function ($f_d(j)$) for drops with radius between 1 μm and 4096 μm (73 categories) is calculated from:

$$\frac{\partial f_d(j)}{\partial t} = -(w - V_r(j))\frac{\partial f_d(j)}{\partial z} - 2\frac{\alpha^2}{a}|w|[f_d(j) - f_{de}(j)]$$

$$+\frac{f_d(j)V_r(j)}{\rho_a}\frac{\partial \rho_a}{\partial z} + \frac{2}{a}u_a[f_d(j) - f_{da}(j)] + \frac{1}{\rho_a}\frac{\partial}{\partial z}\left(\rho_a K\frac{\partial f_d(j)}{\partial z}\right)$$

$$\left(\frac{\partial f_d(j)}{\partial t}\right)_{act} + \left(\frac{\partial f_d(j)}{\partial t}\right)_{CE} + \left(\frac{\partial f_d(j)}{\partial t}\right)_{coal} + \left(\frac{\partial f_d(j)}{\partial t}\right)_{B}, \quad (3)$$

where the coalescence $(\partial/\partial t)_{coal}$, the breakup $(\partial/\partial t)_B$ terms, and the effect of terminal velocity for each category are now included.

The cloud mass density function of particles in the drops with radius between 1 μm and 4096 μm, $g_d(j)$, is calculated from:

$$\frac{\partial g_d(j)}{\partial t} = -(w - V_r(j))\frac{\partial g_d(j)}{\partial z} - 2\frac{\alpha^2}{a}|w|[g_d(j) - g_{de}(j)]$$

$$+\frac{g_d(j)V_r(j)}{\rho_a}\frac{\partial \rho_a}{\partial z} + \frac{2}{a}u_a[g_d(j) - g_{da}(j)] + \frac{1}{\rho_a}\frac{\partial}{\partial z}\left(\rho_a K\frac{\partial g_d(j)}{\partial z}\right)$$

$$\left(\frac{\partial g_d(j)}{\partial t}\right)_{act} + \left(\frac{\partial g_d(j)}{\partial t}\right)_{CE} + \left(\frac{\partial g_d(j)}{\partial t}\right)_{coal} + \left(\frac{\partial g_d(j)}{\partial t}\right)_{B}. \quad (4)$$

Two mass density distribution functions $g_{dCIC}(j), g_{dsCIC}(j)$ are calculated for the classical inorganic ($(NH_4)_2SO_4$) and inorganic+organic ($(NH_4)_2SO_4$+WSOC) CCN in the drops, respectively.

ACPD
4, 591–634, 2004

The time evolution of the mass density distribution functions of particles in the small drops (radius between 0.0041 and 1 μm), $g_{ds}(j)$, is calculated for each category number (j) according to:

$$\frac{\partial g_{ds}(j)}{\partial t} = -w\frac{\partial g_{ds}(j)}{\partial z} - 2\frac{\alpha^2}{a}|w|[g_{ds}(j) - g_{dse}(j)]$$

$$+\frac{2}{a}u_a[g_{ds}(j) - g_{dsa}(j)] + \frac{1}{\rho_a}\frac{\partial}{\partial z}\left(\rho_a K\frac{\partial g_{ds}(j)}{\partial z}\right)$$

$$\left(\frac{\partial g_{ds}(j)}{\partial t}\right)_{act} + \left(\frac{\partial g_{ds}(j)}{\partial t}\right)_{CE}, \quad (5)$$

where $g_{ds}(j)$ are the cloud mass density distribution functions $g_{dslOC}(j)$, $g_{dslOC}(j)$ for the classical inorganic ($(NH_4)_2SO_4$) and inorganic+organic ($(NH_4)_2SO_4$+WSOC) CCN in small drops. Note that in this equation, the coalescence, the breakup terms, and the effect of terminal velocity are not considered.

For drops with radius between 1 and 4096 μm, the time evolution for the mass density functions of chemical species ($g_{dC}(j)$) is given by the equation:

$$\frac{\partial g_{dC}(j)}{\partial t} = -(w - V_r(j))\frac{\partial g_{dC}(j)}{\partial z} - 2\frac{\alpha^2}{a}|w|[g_{dC}(j) - g_{dCe}(j)]$$

$$+\frac{g_{dC}(j)V_r(j)}{\rho_a}\frac{\partial \rho_a}{\partial z} + \frac{2}{a}u_a[g_{dC}(j) - g_{dCa}(j)] + \frac{1}{\rho_a}\frac{\partial}{\partial z}\left(\rho_a K\frac{\partial g_{dC}(j)}{\partial z}\right)$$

$$+\left(\frac{\partial g_{dC}(j)}{\partial t}\right)_{act} + \left(\frac{\partial g_{dC}(j)}{\partial t}\right)_{CE} + \left(\frac{\partial g_{dC}(j)}{\partial t}\right)_{coal} + \left(\frac{\partial g_{dC}(j)}{\partial t}\right)_{B}$$

$$+\left(\frac{\partial g_{dC}(j)}{\partial t}\right)_{\mathrm{aq}} + \left(\frac{\partial g_{dC}(j)}{\partial t}\right)_{diff}. \quad (6)$$

ACPD
4, 591–634, 2004

Here, $g_{dC}(j)$ represents the mass density distribution functions of chemical species $g_{dS(IV)}(j)$, $g_{dS(VI)}(j)$, $g_{dO_3}(j)$, $g_{d|H_2O_2}(j)$, $g_{dHO_2}(j)$, $g_{dHCOOH}(j)$, $g_{dHCHO}(j)$, $g_{dOH}(j)$and $g_{dHMSA}(j)$ and which correspond to S(IV), S(VI), O_3, H_2O_2, peroxyl radical HO_2, total formic acid (HCOOH+$HCOO^-$) total formaldehyde ($H_2C(OH)_2$+HCHO), the hydroxyl radical (OH), and the hydroximethanesulfonate ion HMSA ([$HOCH_2SO_3^{1-}$]) in the drops, respectively.

The equations for the mass density distribution functions of chemical species ($g_{dsC}(j)$) for small drops: $g_{dsS(IV)}(j)$, $g_{dsS(VI)}(j)$, $g_{dsO_3}(j)$, $g_{dsH_2O_2}(j)$, $g_{dsHO_2}(j)$, $g_{dsHCOOH}(j)$, $g_{dsHCHO}(j)$, $g_{dsOH}(j)$ and $g_{dsHMSA}(j)$, have the form:

$$\frac{\partial g_{dsC}(j)}{\partial t} = -w\frac{\partial g_{dsC}(j)}{\partial z} - 2\frac{\alpha^2}{a}|w|[g_{dsC}(j) - g_{dsCe}(j)]$$

$$+\frac{2}{a}u_a[g_{dsC}(j) - g_{dsCa}(j)] + \frac{1}{\rho_a}\frac{\partial}{\partial z}\left(\rho_a K\frac{\partial g_{dsC}(j)}{\partial z}\right)$$

$$+\left(\frac{\partial g_{dsC}(j)}{\partial t}\right)_{act} + \left(\frac{\partial g_{dsC}(j)}{\partial t}\right)_{CE} + \left(\frac{\partial g_{dsC}(j)}{\partial t}\right)_{aq} + \left(\frac{\partial g_{dsC}(j)}{\partial t}\right)_{diff} \quad (7)$$

now the coalescence, breakup terms and the effect of droplet's terminal velocity are not included.

In all the equations, the variables with subscript *e* denote environmental parameters, while subscript *a* refers to values at the perimeter of the cloud, and V_r corresponds to the terminal velocity of drops. The first term on the right-hand side of each equation represents the vertical advection, the second term is the lateral eddy exchange, which is often called turbulent entrainment through the lateral boundary of the cloud, the third term is the effect of divergence of terminal velocities of raindrops, the fourth term is the dynamic entrainment term required to satisfy the mass continuity and the fifth term is the vertical turbulent diffusion. The terms $(\partial/\partial t)_{act}$, $(\partial/\partial t)_{CE}$, $(\partial/\partial t)_{coal}$, $(\partial/\partial t)_B$, $(\partial/\partial t)_{diff}$ and $(\partial/\partial t)_{aq}$ represent the effects of nucleation, condensation and

ACPD
4, 591–634, 2004

evaporation, coalescence, breakup, gas uptake and aqueous phase reactions, respectively. In the equations for aerosols and small droplets, we did not include the third term (effect of divergence due to terminal velocity).

Gas phase species evolve according to:

$$\frac{\partial C_{g,i}}{\partial t} = -w\frac{\partial C_{g,i}}{\partial z} - 2\frac{\alpha^2}{a}|w|(C_{g,i}-C_{ge,i}) + \frac{2}{a}u_a(C_{g,i}-C_{ga,i})$$

$$+\frac{1}{\rho_a}\frac{\partial}{\partial z}(\rho_a K\frac{\partial}{\partial z}C_{g,i}) + (\frac{\partial C_{g,i}}{\partial t})_{diff} \quad (8)$$

where $C_{g,i}$ (i=1,7) is the gas concentration of SO_2, O_3, H_2O_2, HO_2, HCOOH, HCHO and OH in the air. The gas phase rate due to the uptake to or desorption from solution droplets in the category j is given by the expression,

$$\left(\frac{\partial C_{g,i,j}}{\partial t}\right)_{diff} = -\left(\frac{dC_{l,i,j}}{dt}\right)M_g V_d(j) f_d(j) \quad (9)$$

where M_g is the molecular mass of the gas, $V_d(j)$ is the volume of the drops in category $j$and $f_d(j)$ is the cloud number density distribution function and $\left(\frac{dC_{l,i,j}}{dt}\right)$ is calculated according to (Eq. 11). The final bulk mass transfer rate for each i gas due to the uptake (desorption) is calculated by integrating (for both small droplets and drops, 73+48 bins) over all the categories in the form:

$$\left(\frac{\partial C_{g,i}}{\partial t}\right)_{diff} = -\sum_{j=1}^{48}\left(\frac{dC_{l,i,j}}{dt}\right)M_g V_{ds}(j) f_{ds}(j) - \sum_{j=1}^{73}\left(\frac{dC_{l,i,j}}{dt}\right)M_g V_d(j) f_d(j) \quad (10)$$

In Eqs. (1)–(8), t represents time and α^2 is the coefficient for lateral eddy mixing, which is assumed to be 0.1. The vertical eddy diffusion coefficient K is considered constant and the same for all variables and assumed to be 25 m^2/s, and a is the cloud radius that is set equal to 1000 m in our simulations.

ACPD
4, 591–634, 2004

2.3. Chemistry

2.3.1. The influence of CCN organic composition on the critical supersaturation

Following Mircea et al. (2002), we define:

a) the classical inorganic case (CIC), assuming that the CCN are composed only by inorganic compounds, in particular we use ($(NH_4)_2SO_4$).

b) the inorganic + organic case (IOC), when the CCN composition includes inorganic and WSOC.

Because the organic composition of the CCN cannot be attributed to a few major species alone (Facchini, 2001) the organic composition to be used in numerical simulations of cloud physical and chemical processes needs some simplifications. As was pointed out by Saxena and Hildemann (1996), observations regarding the molecular composition of the water-soluble organic fraction are limited. In some studies, only approximately 5 to 20% of the total water-soluble organic carbon was resolved into specific compounds. Decesari et al. (2000), investigated aerosol and fog water samples and found that acidic compounds (mono/dicarboxylic acids) are the dominant WSOC, accounting for an average 59% of soluble organic species.

For maritime aerosols Putaud et al. (2000) reported that dicarboxylic acids of low molecular mass (DA) represent an average 7% of the total mass while polyacidic compounds of higher molecular mass (PACC) constitute 3% of the total mass. In rural aerosols, the fraction of DA increases up to 14%.

Mircea et al. (2002) considered both CIC and IOC CCN composed of 50% by mass of soluble inorganic matter, and the remaining 50% insoluble for the CIC, and 30% insoluble and 20% WSOC for the IOC CCN. They parameterized the DA as an acid with a molecular mass M=100 and number of dissociated ions ν=3 while the polyacidic compounds of higher molecular mass (PACC) was parameterized as fulvic acid having M=732 and ν=5. The soluble inorganic part was considered to be composed by $(NH_4)_2SO_4$(26%) and NH_4NO_3(24%).

In our study we consider 10% soluble inorganic matter, the remaining 90% in the

ACPD
4, 591–634, 2004

CIC is considered to be insoluble material (with a density of 2.5 g/cm^3), while in the IOC, 50% is considered insoluble and 40% WSOC (See Table 1). The WSOC are parameterized as oxalic acid with a molecular mass M=90, and ν=3 because the oxalic acid is generally the most abundant followed by malonic and succinic acids (Kawamura et al., 1996; Yao et al., 2002).

In order to take into account the presence of WSOC in the CCN we used a modified form of the Köhler equation (Mircea et al., 2002):

$$S = \frac{2\sigma M_w}{R_v T \rho_w r} - \frac{3\Phi_s M_w}{4\pi\rho_w r^3} \times \left(\sum_{i\_inorg} \frac{v_i m_i}{M_i} + \sum_{j\_org} \frac{v_j m_j}{M_j} \right) \quad (11)$$

where S is the supersaturation ratio, M_w and ρ_W are the molecular mass and density of water, σ is the surface tension, Φ_s is the osmotic coefficient (Φ_s=1), R_v is the gas constant, T is the temperature, and r is the droplet radius. The number of dissociated ions, soluble mass and molecular mass, respectively of the inorganic and organic components of CCN particles are represented by v_i, m_i, M_i and v_j, m_j, M_j. An ideal solution is assumed ($\rho_s = \rho_W$).

Even though Facchini et al. (1999) found a relationship for the variation of the cloud droplet surface tension (σ in Eq. 11) as a function of dissolved organic carbon concentration, we neglect this dependency in this study.

Table 1 shows the influence of the organic compounds present in the initial CCN, on the critical supersaturation spectrum (CSS) for 13 of the 64 CCN bins used in our simulations. IOC CCN require lower critical supersaturation to activate than CIC CCN for the same dry radius. The smallest IOC CCN (0.0041 μm) becomes activated at 6.61%, while a supersaturation of 17.42% is required to activate the smallest CCN in the CIC. On average for all dry CCN sizes the critical supersaturation in the IOC is a about a factor of 3 smaller than in the CIC.

ACPD
4, 591–634, 2004

2.3.2. Uptake and desorption

The uptake and desorption of the following gas-phase species: sulfur dioxide, (SO_2); hydrogen peroxide, (H_2O_2); peroxyl radical (HO_2); ozone, (O_3); hydroxyl radical, (OH); formaldehyde, (HCHO); formic acid, (HCOOH) for a drop of radius "r" was implemented by means of a quasi analytical solution of the equation:

$$\frac{dC_{l,i,j}}{dt} = \frac{3D_{g,i}f_g}{r^2(j)}(C_{g\infty,i} - \frac{C_{l,i,j}}{K^*_{h,i}RT}) \quad (12)$$

where $C_{g\infty,i}$ (i=1, 7) is the concentration in the gas phase. $C_{l,i,j}$ (i = 1, 7) is the aqueous phase concentration in category j of the corresponding aqueous phase species: S(IV), O_3, H_2O_2, HO_2, total formic acid (HCOOH+$HCOO^-$), total formaldehyde ($H_2C(OH)_2$+HCHO) and the hydroxyl radical (OH). $D_{g,i}$ is the diffusion coefficient for gas species i, f_g the ventilation coefficient for water vapor in air, $K^*_{h,i}$ the modified Henry's law coefficient for gas species i, that depends on pH, R_v the universal gas constant and T the temperature.

The reaction with O_3 plays an important role both as a sink of gas-phase SO_2 and as a source of cloudwater acidification as long as the pH of the droplets exceeds about 4. On the other hand, H_2O_2 is very soluble in water and under typical ambient conditions its aqueous phase concentration is approximately six orders of magnitude higher than that of dissolved ozone.

At every time step in the simulation the aqueous concentration $C_{l,i}$, is calculated by using the analytical expression

$$C_{l,i,j}(t) = (C_{l0,i,j} - K^*_{h,i}RTC_{g\infty,i})e^{((-3D_{g,i}/r^2(j)K^*_{h,i}RT)t)} + K^*_{h,i}RTC_{g\infty,i} \quad (13)$$

and the method described in detail in AR2002. The gas phase concentrations are updated at every time step using the aqueous phase concentrations calculated in Eq. (12).

ACPD
4, 591–634, 2004

2.3.3. Aqueous phase chemistry

The equilibrium aqueous phase chemistry and dissociation constants for inorganic and organic species are listed in Tables 2 and 3.

The S(IV) is oxidated by H_2O_2, O_3 and $(OH)_{aq}$ in order to generate S(VI). The production of formic acid from hydrated formaldehyde, that is oxidized by the hydroxyl radical in the aqueous phase $(OH)_{aq}$, is also calculated. HSO_3^- reacts with disolved formaldehyde to produce the hydroximethanesulfonate ion (HMSA), that is a member of the S(IV) family. The HO_2 cycle is also included in the simulations. The aqueous phase photochemistry of the hydrogen peroxide at a constant rate is also considered (equinox conditions with a cloud transmissivity factor of 0.5).

The Livermore Solver for Ordinary Differential Equations (DLSODE) was used to solve equations listed in Tables 2 and 3. The method solves the initial-value problem for stiff or nonstiff systems of first-order ODE's. The disadvantage of this method, like other Gear (1971) type solvers, is that it needs to solve large matrices of partial derivatives, hence limiting its use in three dimensional or large scale models (Barth et al., 2003).

2.3.4. pH calculation

The resulting acidity defined by pH=-log[H^+] is derived from the electroneutrality condition that in the general case is:

$$\sum \gamma_i n_i = 0 \tag{14}$$

where n_i is the concentration of an ion of charge γ_i. In particular, for the situation studied here:

$$[NH_4^+] + [H^+] = [OH^-] + [HSO_3^-] + 2[SO_3^{2-}] + [HSO_4^-] + 2[SO_4^{2-}] + [HCOO^-]$$

$$+[HD^-] + 2[D^{2-}] + [HOCH_2SO_3^-] + [O_2^-]. \tag{15}$$

ACPD
4, 591–634, 2004

A polynomial equation in $[H^+]$ is then obtained in the form:

$$[NH_4^+] + [H^+] = \frac{k_w}{[H^+]} + [S(IV)] \frac{(K_1[H^+] + 2K_1K_2)}{([H^+]^2 + K_1[H^+] + K_1K_2)} + [S(VI)] \frac{(2K_3 + [H^+])}{(K_3 + [H^+])} \cdot$$

$$+ [HCOOH] \frac{K_{HCOOH}}{([H^+] + K_{HCOOH})} + [H_2D] \frac{(K_{D1}[H^+] + 2K_{D1}K_{D2})}{([H^+]^2 + K_{D1}[H^+] + K_{D1}K_{D2})} + [HOCH_2SO_3^-]$$

$$+ [HO_2] \frac{K_{HO_2}}{([H^+] + K_{HO_2})} \quad (16)$$

In this equation, K_1, K_2 and K_3 and k_w are the dissociation equilibrium constants for the S(IV), S(VI) and water, respectively, and K_{HCOOH1}, K_{D1}, K_{D2}, and K_{HO_2} are the constants for the formic, oxalic acids and HO_2, respectively. As we pointed out in the introduction, the role of WSOC in the pH spectrum of precipitation, is beyond the scope of this study and wasn't included in the analysis. Thus, the pH in our simulations is calculated for each drop category for the CIC case, and Eq. (15) without the term for the oxalic acid was actually used.

3. Initial conditions

3.1. CCN distributions

Simulations were performed with two maritime distributions for the classic inorganic (CIC) and the inorganic+organic cases (IOC). Each distribution consists of a superposition of two log-normal CCN distributions with the same parameters as in AR2002.

Although Hoppel et al. (1990) reported total concentrations above 200 cm^{-3} in the Atlantic Ocean, the total CCN concentration in our simulations is 100 cm^{-3}, typical of

ACPD
4, 591–634, 2004

maritime conditions. When the concentration was increased, a simulated cloud with an unrealistic long lifetime was obtained. A similar situation was reported by Takahashi (1976), using the same dynamics, when he observed an overestimation of cloud lifetime for the continental case. Because of that, an increase in the CCN concentrations due to the anthropogenic activity was not considered in our simulations. Therefore, the total CCN concentration is 100 cm^{-3} in the contaminated case. The accumulation mode concentration of the CCN spectra was set equal to 50 cm^{-3}.

3.2. Initial vertical distributions of thermodynamic parameters and gaseous species

Chameides (1984) set very low initial concentrations (10^{-4} ppb) of formic acid. For realistic atmospheric conditions, initial $HCOOH_{(g)}$ concentrations are often higher, between 0.03–1.7 ppb; (Chebbi and Carlier, 1996) and are close to those of $HCHO_{(g)}$. Granby and Christensen (1997) reported urban winter mean concentrations of 0.80±0.30 ppb for formic acid and 2.6±0.7 ppb for formaldehyde, while at a semi rural site concentrations were 0.6±0.3 and 0.9±0.5, respectively.

Arlander et al. (1990) reported mesaurements of the background levels of trace organic species in the remote marine troposphere. For the northern hemisphere Pacific Ocean the mean formic acid concentration was 0.80±0.30 ppb, while in the southern hemisphere was 0.22±0.13 ppb. For the northern hemisphere Indian Ocean the mean concentration was 0.75± 0.24 ppb. In general formic acid gas phase concentrations in maritime zones are in the range between 0.03–1.7 ppb and 0.1–13.4 ppb for the formaldehyde (Arlander et al., 1990 and references therein). In our study, a 1ppb initial concentration at the surface for both formic acid and formaldehyde was chosen.

Table 4 presents the initial concentrations at the surface for all the gaseous species. Hidroxyl radical concentration has a large variability during the day, but in this study was set equal to 5×10^{-4} ppb following Ridley et al. (1990). A high background concentration of SO_2 (20 ppb) is assumed to simulate anthropogenic emissions from the petroleum platforms following Ramos (1997). All gas concentrations are assumed to decrease exponentially with height as in AR2002.

ACPD
4, 591–634, 2004

The initial sounding corresponds to the city of Veracruz, located on the coast of the Gulf of Mexico (see AR2002). A small updraft is imposed to start convection in the layer below 2 km, with a maximun value of 1 ms^{-1} at a height of 1 km. The duration of the simulations is 80 min.

4. Results

4.1. Sensitivity to CCN composition

The evolution of dynamical and microphysical cloud characteristics was discussed in detailed in AR2002. We do not include some tests regarding cloud parameters as cloud radius here. However, some sensitivity tests to prescribed cloud parameters (i.e. cloud radius) can be found in Alfonso et al. (1998).

A summary of the results obtained for the CIC and IOC simulations is presented in Table 5. Both experiments show cloud top at about 6 km. The differences in maximum vertical velocity are not significant, but the maxima were obtained at different times in the evolution. The more pronounced differences between the two runs are evident in the droplet concentration, presented in Fig. 1, as a function of height after 44 min of simulation. In general, the droplet concentration is smaller in the CIC by 35% and these differences have an effect in the development of precipitation. Precipitation concentration of 1 g kg^{-1} reached the ground after 60 min of simulation in the CIC, and after 63 min in the IOC. In our simulations, we only tested the influence of the concentration in the precipitation development. We did not change any other parameters of the CCN distribution like the dispersion and the mean radius.

The maximum supersaturations are larger in the CIC simulation, due to the smaller maximum droplet concentrations (S=3.4% in the CIC vs. 2.9% in the IOC).

ACPD
4, 591–634, 2004

4.2. Calculations of pH

4.2.1. High ambient SO_2 concentration (20 ppb)

Four simulations (summarized in Table 6) were performed in order to test the influence of the aqueous phase chemistry and the initial concentration of formic acid in the pH droplet spectra, the CCN composition on all the simulations is the CIC composition ($(NH_4)_2SO_4$). These simulations are summarized in Table 6.

Cases with no aqueous-phase oxidation (NAPR1 and NAPR0)

Since no aqueous phase oxidation is ocurring, the process that causes the increase in droplet's acidity in the NAPR1 and NAPR0 simulations is the direct transfer of acidic CCN and gases to droplets (the diffusion of SO_2, and the diffusion and dissociation of HCOOH). The vertical variation of the gas concentration in air for HCHO, HCOOH, H_2O_2 is displayed in Fig. 2 after 44 min of simulation. Due to the high solubility constant for H_2O_2, its gas concentrations in air are lowest since it diffuses faster than HCHO and HCOOH.

The pH spectra obtained at three different incloud levels are displayed in Fig. 3. In the NAPR1 case droplets become less acidic with increasing height because they tend to be in equilibrium with the environmental gas concentrations, that decrease with height. As a result, aqueous S(IV) and HCOOH concentration decrease with height and the pH increases. Droplets larger than 200 μm at 2000 and 300 m are mainly produced by collisions of numerous small drops that have scavenged SO_2 and HCOOH according to Henry's law at lower levels where gas concentrations are larger. They are more acidic because they desorb SO_2 and HCOOH less efficiently than smaller droplets and they have larger concentrations than equilibrium S(IV) and $(HCOOH)_{aq}$ concentrations at that height. At cloud base (1000 m) smaller droplets are in equilibrium with gas concentrations and are more acidic than larger drops.

An aditional simulation (NAPR0) with no initial concentration of $(HCOOH)_g$ was per-

ACPD
4, 591–634, 2004

formed to test the influence of the gas phase concentration of formic acid in the droplets acidity. The differences between the two simulations are shown in Fig. 4 for a height of 2000 m. A lowering of the pH by 0.1 pH units (about 2% reduction) is observed for every drop category when gas phase formic acid is present (compare curves marked as NAPR0 and NAPR1).

The contribution of monocarboxylic and dicarboxylic acids to bulk rain acidity was estimated by Kawamura et al. (1996) from experimental data. They reported that, although nitric and sulfuric acid are the principal contributors to H^+ ion concentration in acid rain, organic acids lower the pH of rainwater between 0.1 and 1.9 pH units. Our results considering high SO_2 ambient concentration are consistent with their low estimate of pH change due to organic acids.

Cases with aqueous-phase oxidation (APR1 and APR0)

In the APR1 simulation, chemical reactions decrease the concentration of dissolved SO_2, H_2O_2, O_3, HCHO and OH to produce S(VI), HCOOH, HMSA, enhance cloud water acidity and perturb the equilibrium aqueous phase concentrations of the mentioned species. Consequently, a gas phase adjustment takes place enhancing the uptake of species that are depleted in the aqueous phase.

A significant reduction in the gas-phase concentrations compared to the NAPR1 case is observed, as for example for the H_2O_2, SO_2 and OH (see Figs. 5, 6 and 7) after 44 min of simulation. A comparison between pH spectrum obtained for the NAPR1 and APR1 cases is given in Fig. 4, where a pH reduction for the APR1 case up to 0.5 units is observed for a model time of 44 min at 2000 m.

There are some differences in the spectral behaviour of the aqueous phase species. As SO_2 is taken up by cloud water as S(IV) and is converted to S(VI) by oxidizing gases in the aqueous phase (H_2O_2, O_3 and OH), the production of acid from SO_2 takes some time, and is most concentrated in the largest, oldest drops, that have lived the longest time. On the other hand, the scavenged SO_2 gas is redistributed to the large end

ACPD
4, 591–634, 2004

of the spectrum as a consequence of the collision coalescence process. This can be deduced from Fig. 8, where a decrease in the S(IV) concentration with radius is observed for droplets larger than 80 μm, as a result of S(IV) oxidation. The S(VI) is more concentrated in large drops in comparison with small droplets, because of the microphysical conversion due to the collision-coalescence process.

Because of its high solubility, the $(HCOOH)_{aq}$ resulting from the uptake of $(HCOOH)_g$ is confined mainly to the small drops both at cloud base (1000 m) and at 2000 m at 44 min (see Fig. 9). The reduction of the aqueous phase concentration with height is a result of the exponential decrease in environmental gas concentrations. Then the gas is transferred to the large end of the spectrum (500–1000 μm) by droplet collisions and coalescence. The aqueous phase concentration is larger at the small end of the spectrum for the case with aqueous phase reactions (APR1). Aqueous phase reactions can explain higher formic acid concentrations at the small end of the spectrum in APR1 than in NAPR1 case. In both cases, HCOOH uptake takes place. Thus only aqueous phase oxidation of formaldehyde can explain the differences, since the oxidation of HCHO is more important at the small end when gas uptake is more efficient.

A similar situation was explored by Wurzler et al. (1995) for only inorganic acids, indicating that the scavenging behaviour of nitrate and of sulfate is significant different, because nitric acid in cloud water is formed directly on uptake of HNO_3 gas, and sulfuric acid is formed after the reaction with oxidizing agents such as H_2O_2. They found also that nitrate resulting from uptake of HNO_3 is confined mainly to small drops, whereas sulfate is most concentrated at the large end of the spectrum. Although the $(HCOOH)_{aq}$ is also destroyed by the reaction with the $(OH)_{aq}$, in this study we observe a behaviour similar to the one discussed by Wurzler et al. (1995).

Even though the production of sulfuric acid is the most important factor in generating droplet's acidity, there is a contribution due to the diffusion and generation of formic acid in the droplets. As seen in Fig. 4, there is a reduction in pH (between 0.1 and 0.15 pH units) in the entire spectrum.

ACPD
4, 591–634, 2004

4.2.2. Low ambient SO_2 concentration (1 ppb)

Again four simulations were performed in order to test the importance of the uptake and formic acid production in drop acidity, listed in Table 6.

a) Cases with no aqueous-phase oxidation (NAPR1 and NAPR0)

In the NAPR1 simulation, the diffusion and dissociation of HCOOH is very important in generationg the acidity of the droplets, as seen in Fig. 10. The pH variation is large, and a decrease from a pH in the 5.2–5.5 range for the NAPR0 to a pH of 5 for the NAPR1 is observed. The presence of HCOOH increases the acidity drastically (NAPR1), specially for smaller drops that have a more efficient uptake. The acidity increases with radius for the NAPR0 due to higher concentrations of S(IV) at the large end. This is a consequence of the microphysical conversion due to collision-coalescence process.

b) Cases with aqueous-phase oxidation (APR1 and APR0)

In the APR0 simulation, the results show an increase of the acidity at the large end, because S(VI) is more concentrated in large drops as a result of the microphysical conversion due to coalescence. For the APR1 case, less pronounced increase with radius is observed, due to the uptake of HCOOH, that is confined mainly to the small drops. In the high ambient SO_2 concentration case (20 ppb), the behaviour of the pH spectrum at the small end was modulated by the S(IV) and the pH decreased from 4.9 to 4.5, approximately. In the low ambient SO_2 concentration case, there is an increase in acidity due to the HCOOH uptake (from 0.2 to 0.5 pH units). Therefore, in cases where HCOOH and SO_2 have similar gaseous concentrations, the resulting acidity is clearly affected by the uptake and production of the organic acid.

ACPD
4, 591–634, 2004

5. Conclusions

The microphysical-chemical cloud model reported in AR2002 was used to test the influence of WSOC CCN composition, solubility, and background inorganic+organic gas concentrations in the development of cloud and precipitation, and in the pH spectral evolution. In our previous study, primary emitted particles were assumed to have a large fraction (90%) composed of non-soluble material. In the present study we consider that 40% of the total mass consists of WSOC (represented by oxalic acid).
The conclusions can be summarized as follows:

a) Considering the presence of WSOC in the CCN:

- The differences in total droplet concentrations between the CIC and IOC were significant, with lower droplet concentrations for the CIC and an earlier development of precipitation.
- The presence of DA in CCN reduces the critical supersaturation by a factor of 3.

b) Considering the impact of formic acid in the final pH of rain:

- When no aqueous phase oxidation is allowed, dissolved species in droplets tend to be in equilibrium with the environmental gas concentrations, that are assumed to decrease with height in this study. Larger droplets (formed by collisions and coalescence of smaller ones) have higher concentrations than equilibrium S(IV) and $(HCOOH)_{aq}$ concentrations at upper cloud levels. Larger droplets desorb SO_2 and HCOOH less efficiently than smaller ones. The result is an increase in the acidity at the large end of the spectrum. A reduction of the pH in the range from 0.05 to 0.15 pH units was observed due to the diffusion of HCOOH.
- The uptake of HCOOH is confined mainly to the small drops, due to its high solubility, with formic acid formed directly in the cloud water from the dissolved gas.

ACPD
4, 591–634, 2004

- The depletion of S(IV) by the oxidation reactions with H_2O_2, O_3 and OH is observed and its concentration decreases with droplet size at upper levels.
- The reaction of S(IV) with the oxidizing agents (H_2O_2, O_3 and OH) generates S(VI) and it is most concentrated in the largest, oldest drops, that have had more time for reaction, and because of the microphysical conversion by collision-coalescence.
- In the high ambient SO_2 concentration case, a reduction in pH (in the range from 0.05 to 0.15 pH units) was observed due to diffusion and aqueous phase production of HCOOH in the case with aqueous phase oxidation. This reduction is less pronounced at the large end of the spectrum, with oldest droplets that have produced more $(HCOOH)_{aq}$ from hydrated formaldehyde.
- The small reductions in the pH due to diffusion and generation of formic acid in the aqueous-phase are associated with the high ambient (20 ppb) SO_2 concentration.
- A more pronounced increase in the acidity is observed (from 0.2 to 0.5 pH units) up to 10% as a result of the uptake and production of formic acid in the low (1 ppb) SO_2 concentration case.
- When ambient gaseous concentration of SO_2 and HCOOH are comparable, the importance of formic acid in determining the pH is clearly observed.

Acknowledgements. This study was partially funded through grants from Conacyt (#32528) and (#33319) and DGEP. The authors would like to thank S. Madronich and M. Barth from NCAR and M. Moya from UNAM, for useful suggestions and discussions.

References

Alfonso, L. A., Martínez, D., and Pérez, C. A.: Numerical simulations of tropical convective clouds over Cuba using a one-dimensional and time dependent model, Atmos. Res., 47–48, 343–354, 1998.

Alfonso, L. and Raga, G. B.: Estimating the impact of natural and anthropogenic emissions on cloud chemistry, Part I, Sulfur cycle, Atmos. Res., 62, 33–55, 2002.
Arlander, D. W., Cronin, D. R., Farmer, J. C., Menzia, F. A., and Westberg, H. H.: Gaseous oxygenated hydrocarbons in the remote marine troposphere, J. Geophys. Res., 95, D10, 16 391–16 403, 1990.
Anbar, M. and Neta, P.: A compilation of specific bimolecular rate constants for the reactions of hydrated electrons. Hydrogen atoms and hydroxyl radicals with inorganic and organic compounds in aqueous solutions, Int. J. Appl. Radiat. Isotopes, 18, 493–523, 1967.
Asai, T. and Kasahara, A.: A theoretical study of compensating downward motions associated with cumulus clouds, J. Atmos. Sci., 24, 487–496, 1967.
Barth, M. C., Skamarock, W. C., and Stuart, A. L.: The influence of cloud processes on the distribution of chemical species for the 10 July 1996 STERAO/Deep Convection Storm, Proceedings of the 13 International Conference on Clouds and Precipitation, Nevada, USA, 960–963, 2000.
Barth, M. C., Sillman, S., Hudman, R., Jacobson, M. Z., Kim, C. H., Monod, A., and Liang, J.: Summary of the cloud chemistry modeling intercomparison: Photochemical box model simulation, J. Geophys. Res., 108, D7, AAC 5-1, AAC 5-19, 10.1029/2002JD002673, 2003.
Berry, E.: Cloud droplet growth by collection, J. Atmos. Sci., 24, 688–701, 1967.
Bielski, B. H. J.: Reevaluation of the spectral and kinetic properties of HO_2 and O_2^- free radicals, Photochem. Photobiol., 28, 645–649, 1978.
Bothe, E. and Schulte-Frohlinde, D.: Reaction of dihydroxymethyl radical with molecular oxygen in aqueous solution, Anorg. Chem. Org. Chem., 35, 1035–1039, 1980.
Chameides, W. L.: The photochemistry of a remote marine stratiform cloud, J. Geophys. Res., 89, 4739–4755, 1984.
Chebbi, A. and Carlier, P.: Carboxylic acids in the troposphere, occurrence, sources, and sinks: A review, Atmos. Environ., 30, 4233–4249, 1996.
Corriga, C. E. and Novakov, T.: Cloud condensation nucleus activity of organic compounds: a laboratory study, Atmos. Environ., 33, 2661–2668, 1999.
Christensen, H. Sehested, K., and Corfitzen, H.: Reaction of hydroxyl radicals with hydrogen peroxide at ambient and elevated tempeartures, J. Phys., 77, 1111–1116, 1982.
Cruz, C. N. and Pandis, S. N.: A study of the ability of pure secondary organic aerosol to act as cloud condensation nuclei, Atmos. Environ., 31, 2205–2214, 1997.
Decesari, S., Facchini, M. C., Fuzzi, S., and Tagliavini, E.: Characterization of water soluble

ACPD
4, 591–634, 2004

organic compounds in atmospheric aerosol: a new approach, J. Geophys. Res., 105, 1481–1489, 2000.
Facchini, M. C.: Organic compounds in clouds: Present knowledge and future perspectives, Newsletter of the International Global Atmospheric Chemistry Project, 23, 10–13, 2001.
Facchini, M. C., Mircea, M., Fuzzi, S., and Charlson, R. J.: Cloud albedo enhancement by surface-active organic solutes in growing droplets, Nature, 401, 257–259, 1999.
Feingold, G. and Chuang, P. Y.: Analysis of the influence of film forming compounds on droplet-growth: implications for cloud microphysical processes and climate, J. Atmos. Sci., 59, 2006–2018, 2002.
Gear, C. W.: Numerical Initial Value Problems in Ordinary Differential equations, Prentice Hall, Englewood Cliffs, NJ, 1971.
Graedel, T. E. and Weschler, C. J.: Chemistry within aqueous atmospheric aerosols and Raindrops, Rev. Geophys., 19, 505–539, 1981.
Granby, K. and Christensen, C. C.: Urban and semirural observations of carboxylic acids and Carbonyls, Atmos. Environ., 31, 1403–1415, 1997.
Hegg, D. A., Gao, S., and Jonsson, H.: Measurements of selected dicarboxylic acids in marine cloud water, Atmos. Res., 62, 1–10, 2002.
Helas, G., Andreae, M. O., and Hartmann, W. R.: Behavior of atmospheric formic and acetic acid in the presence of hydrometeors, J. Atmos. Chem., 15, 101–115, 1992.
Hoffmann, M. R. and Calvert, J. G.: Chemical transformation Modules for Eulerian Acid Deposition Models, Volume 2, The Aqueous-Phase Chemistry, EPA/600/3-85/017, US Environmental Protection Agency, Research Triangle Park, NC, 1985.
Hoppel, W. A., Fitzgerald, J. W., Frick, G. M., Larson, R. E.: Aerosol size distributions and optical properties found in the maritime boundary layer over the Atlantic Ocean, J. Geophys. Res., 95, 3659–3686, 1990.
Huie, R. E. and Neta, P.: Chemical behaviour of SO_3^- and SO_5^- radicals in solution, J. Phys. Chem., 88, 5665–5669, 1984.
Kawamura, K., Steinberg, S., and Kaplan, I. R.: Concentrations of monocarboxylic and dicarboxylic acids and aldehydes in southern California wet precipitations: Comparison of urban and nonurban samples and compositional changes during scavenging, Atmos. Environ., 30, 1035–1052, 1996.
Klanning, U. R., Sehesfeld, K., and Holcman, J.: Standard Gibbs energy of formation of the hydroxyl radical in aqueous solution, J. Phys. Chem., 89, 5, 760–763, 1985.

Lelieveld, J. and Crutzen, P. J.: The role of clouds in tropospheric photochemistry, J. Atmos. Chem., 2, 229–267, 1991.
Likens, G. E., Edgerton, E. S., and Galloway, J. N.: The composition and deposition of organic carbon in precipitation, Tellus, 35B, 16–24, 1983.
Löflund, M., Kasper-Giebl, A., Schuster, B., Giebl, H., Hitzenberger, R., and Puxbaum, H.: Formic, acetic, oxalic, malonic and succinic acid concentrations and their contribution to organic carbon in cloud water, Atmos. Environ., 36, 1553–1558, 2002.
McArdle, J. V. and Hoffmann, M. R.: Kinetic and mechanisms of the oxidation of aquated sulfur dioxide by hydrogen peroxyde al low pH, J. Phys. Chem., 87, 5425–5429, 1983.
Mircea, M., Facchini, M. M., Decesari, S., Fuzzi, S., and Charlson, R. J.: The influence of organic aerosol component on CCN supersaturation spectra for different aerosol types, Tellus, 54B, 74–81, 2002.
National Bureau of Standards: Selected values of chemical thermodynamic properties, 1, N.B.S. Tech. Note, 270-1, 124, 1965.
Novakov, T. and Penner, J. E.: Large contribution of organic aerosols to cloud-condensation-nuclei Concentrations, Nature, 365, 823–826, 1993.
Pruppacher, H. R. and Klett, J. D.: Microphysics of clouds and precipitation, Kluwer Academic Publishers, 1997.
Putaud, J. P., Van Dingenen, R., Mangoni, M., Virkula, A., Raes, F., Maring, H., Prospero, J. M., Swielicki, E., Berg, O., Hillamo, R., and Makela, T.: Chemical clossure and assesment of the origin of the submicron aerosol in the maritime boundary layer and the free troposphere at Tenerife during ACE-2, Tellus, 52B, 141–168, 2000.
Ramos, L. Y.: Evaluación de SO_2 y NO_2 en puntos contaminantes por la Industria Petrolera en el Estado de Tabasco, Tesis de Lic. En Química, 107, 1997.
Ridley, B. A., Madronich, S., Chatfield, R. B., Walega, J. G., and Shetter, R. E.: Measurements and model simulations of the photostationary state durinf the Mauna Loa observatory photochemistry experiment: Implications for radical concentrations and ozone production and loss rates, J. Geophys. Res., 97, 10 375–10 388, 1992.
Saxena, P. and Hildemann, L. M.: Water soluble organics in atmospheric particles: A critical review of the literature and application of thermodynamics to identify candidate compounds, J. Atmos. Chem., 24, 57–109, 1996.
Scholes, G. and Wilson, R. L.: γ radiolysis of aqueous thymine solutions. Determination of relative reaction rates of OH radicals, Trans. Faraday Soc., 63, 2982–2993, 1967.

Sehested, K., Rasmussen, O. L., and Fricke, H.: Rate constants for OH with HO_2, O_2^-, and H_2O_2 from hydrogen preoxide formation in pulse irradiated oxygenated water, J. Phys. Chem., 72, 626–631, 1968.
Sehested, K., Holeman, J., and Hart, E. J.: Rate constants and products of the reaction of O_2^-, and H with ozone in aqueous solutions, Adv. Environ. Sci. Eng., 4, 1–45, 1983.
Seinfeld, J. H. and Pandis, S. N.: Atmospheric Chemistry and Physics, Jonh Wiley & Sons, 1326, 1998.
Sempere, R. and Kawamura, K.: Comparative distributions of dicarboxylic acids and related polar compounds in snow, rain and aerosols from urban atmosphere, Atmos. Environ., 28, 449–459, 1994.
Staehelin, J., Buhler, R. E., and Hoigne, J.: Ozone decomposition in water studied by pulse radiolysis, 2. OH and HO_4 as chain intermediates, J. Phys. Chem., 88, 5999–6004, 1984.
Takahashi, T.: Warm rain, giant nuclei and chemical balance in a numerical model, J. Atmos. Sci., 33, 269–286, 1976.
Yao, X., Fang, M., Chan, C. K.: Size distributions and formation of dicarboxylic acids in atmospheric particles, Atmos. Environ., 36, 2099–2017, 2002.
Wurzler, S., Flossman, A. I., Pruppacher, H. R., and Schwartz, S. E.: The scavenging of nitrate by clouds and precipitation, J. Atm. Chem., 20, 259–280, 1995.

ACPD
4, 591–634, 2004

Table 1. Critical supersaturations for aqueous solution drops containing CIC and IOC aerosols. DA is a dicarboxylic acid of low molecular mass (oxalic acid), and INS the insoluble fraction.

Aerosol type		CIC			IOC		
Composition		$(NH_4)_2SO_4$	DA	INS	$(NH_4)_2SO_4$	DA	INS
Fraction of the total aerosol mass (%)		10	0.0	90	10	40	50
category	Dry particle radius (μm)	Critical supersaturation (%)			Critical supersaturation (%)		
1	0.0041	17.4263			6.61497		
5	0.0065	8.71319			3.30748		
10	0.0116	3.66344			1.39062		
15	0.0206	1.54029			0.58468		
25	0.0656	0.27228			0.10335		
30	0.1168	0.11448			0.04345		
35	0.2082	0.04813			0.01827		
40	0.3710	0.02023			0.00768		
45	0.6612	0.00850			0.00322		
50	1.1781	0.00357			0.00135		
55	2.0992	0.00150			0.00057		
60	3.7403	0.00063			0.00024		
64	5.9374	0.00031			0.00012		

ACPD
4, 591–634, 2004

Table 2. **(a)** Equilibrium reactions (Henry's Law Equilibria). **(b)** Dissociation constants. **(c)** Dissociation constants. **(d)** Aqueous-phase species.

(a)

Reaction	$K_{H,298\,(M\,atm^{-1})}$	$\Delta H_{298}/R$	Reference
$(SO_2)g \leftrightarrow (SO_2)_{aq}$	1.2	−3135	Hoffmann and Calvert (1985)
$(O_3)_g \leftrightarrow (O_3)_{aq}$	1.15×10^{-2}	−2560	NBS
$(H_2O_2)_g \leftrightarrow (H_2O_2)_{aq}$	9.7×10^{4}	−6600	NBS
$(HO_2)_g \leftrightarrow (HO_2)_{aq}$	9×10^{3}	−6600	Bielski (1978)
$(OH)_g \leftrightarrow (OH)_{aq}$	25	−5200	Klanning et al. (1985)
$(HCHO)_g \leftrightarrow (CH_2(OH)_2)_{aq}$	7×10^{3}	−6425	NBS
$(HCOOH)_g \leftrightarrow (HCOOH)_{aq}$	3.7×10^{3}	−5700	NBS

(b)

Reaction	$K_{H,298}$ (M)	$\Delta H_{298}/R$	Reference
$(SO_2)_{aq} \leftrightarrow HS0_3^- + H^+$	1.7×10^{-2}	−2090	NBS
$HSO_3^- \leftrightarrow H^+ + SO_3^{2-}$	6×10^{-8}	−1120	NBS
$(HO_2)_{aq} \leftrightarrow H^+ + O_2^-$	2×10^{-5}	0	Bielski (1978)
$(HCOOH)_{aq} \leftrightarrow HCOO^- + H^+$	1.8×10^{-4}	1500	Helas et al. (1992)

(c)

Acid	K_1 (M)	K_2 (M)	Reference
Oxalic	5.9×10^{-2}	6.4×10^{-5}	Kawamura et al. (1996)

ACPD
4, 591–634, 2004

Table 2. Continued.

(d)

$S(IV)=SO_2 + HSO_3^- + SO_3^{2-}$
$S(VI)=SO_4^{2-} + HSO_4^- + H_2SO_4$
$HCOOH + HCOO^-$
$H_2C(OH)_2 + HCHO$
$HOCH_2SO_3^{1-}$
$HO_2 + O_2^-$
H_2O_2
O_3
OH

ACPD
4, 591–634, 2004

Table 3. **(a)** Aqueous phase reactions. Oxygen-hydrogen chemistry. **(b)** Aqueous phase reactions. Organic chemistry. **(c)** Aqueous phase reactions. Sulfur chemistry.

Reaction	Kinetic constant ($M^{-n+1}\ s^{-1}$)	Reference
(a)		
$H_2O_2 + h\nu \rightarrow 2OH$	1.4×10^{-5}	Graedel and Weschler (1981)
$O_3 + h\nu + H_2O \rightarrow H_2O_2 + O_2$	6.0×10^{-5}	Graedel and Weschler (1981)
$OH + O_2^- \rightarrow OH^- + O_2$	1.0×10^{10}	Sehested et al. (1968)
$OH + H_2O_2 \rightarrow H_2O + HO_2$	2.7×10^{7}	Christensen et al. (1982)
$HO_2 + HO_2 \rightarrow H_2O_2 + O_2$	8.6×10^{5}	Bielski (1978)
$HO_2 + O_2^- \rightarrow H_2O_2 + O_2 + OH^-$	1.0×10^{8}	Bielski (1978)
$OH + O_3 \rightarrow HO_2 + O_2$	2×10^{9}	Staehelin et al. (1984)
$O_2^- + O_3 + H_2O \rightarrow OH + 2O_2 + OH^-$	1.5×10^{9}	Sehested et al. (1983)
$OH + OH \rightarrow H_2O_2$	5.2×10^{9}	Lelieveld and Crutzen (1991)
(b)		
$H_2C(OH)_2 + OH \rightarrow HCOOH + HO_2 + H_2O$	2×10^{9}	Bothe and Schulte-Frohlinde (1980)
$HCOOH + OH \rightarrow H_2O + CO_2 + HO_2$	2×10^{8}	Scholes and Wilson (1967)
$HCOO^- + OH \rightarrow HO_2 + CO_2 + OH^-$	2.5×10^{9}	Anbar and Neta (1967)
(c)		
$S(IV) + H_2O_2 \rightarrow S(VI) + H_2O$	7.45×10^{7}	McArdle and Hoffmann (1983)
$HSO_3^- + OH \rightarrow OH^- + 2H^+ + SO_4^{2-} + SO_4^-$	4.5×10^{9}	Huie and Neta (1984)
$S(IV) + O_3 \rightarrow S(VI) + O_2$	2.4×10^{4}	Hoffmann and Clavert (1985)

ACPD
4, 591–634, 2004

Table 4. Gas-phase chemical species and initial concentrations at the surface.

Gas-phase species	Initial concentrations at the surface (ppb)
SO_2 (High ambient conc.)	20
SO_2 (Low ambient conc.)	1
HO_2	1×10^{-2}
H_2O_2	1
O_3	100
OH	5×10^{-4}
HCHO	1
HCOOH	1

ACPD
4, 591–634, 2004

Table 5. Results obtained for the CIC and IOC experiments.

Experiment	CIC	IOC
Max vertical velocity (m s^{-1})	10.03	10.33
Time (min) and height (m)	43, 3600	47, 3800
Maximum concentration (droplets + raindrops) (cm^{-3})	74,6	119.4
Mean diameter (mm)	10.39	9.21
Time (min) and height (m)	33, 2000	29.5, 20000
Precipitation reaching ground (1g kg^{-1}) after time (min)	60	63
Maximum supersaturation (%)	3.4	2.9
Time (min) and height (m)	50, 4500	53, 4900

ACPD
4, 591–634, 2004

Table 6. Simulations performed for high (20 ppb) and low (1 ppb) ambient SO_2 concentrations.

	No aqueous phase oxidation		With aqueous phase oxidation	
	Initial $(HCOOH)_g$ concentration at the Earth's surface (ppb)		Initial $(HCOOH)_g$ gas concentration at the Earth's surface (ppb)	
	1	0	1	0
Aerosol composition	CIC: $(NH_4)_2SO_4$ (10% fraction of the total aerosol mass)			
Simulation	NAPR1	NAPR0	APR1	APR0

ACPD
4, 591–634, 2004

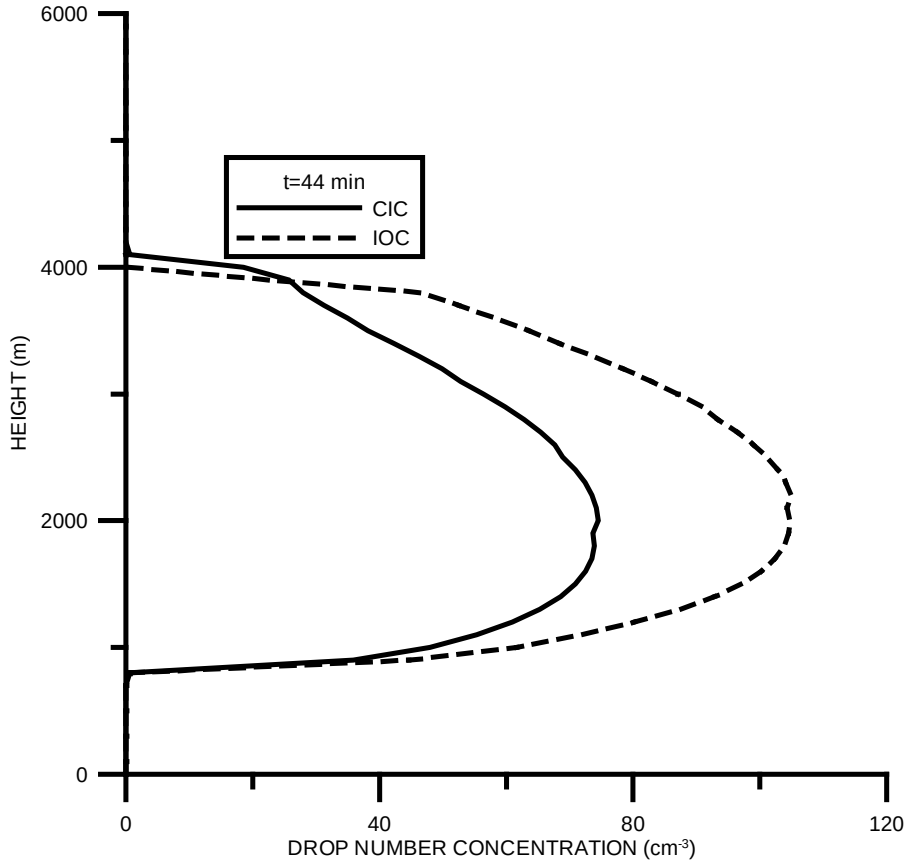

Fig. 1. Droplet number concentration (cm^{-3}) as a function of height for the classical inorganic case (CIC) and inorganic+organic case (IOC) simulations after 44 min of simulation.

ACPD
4, 591–634, 2004

Estimating the impact of natural and anthropogenic emissions

L. Alfonso and G. B. Raga

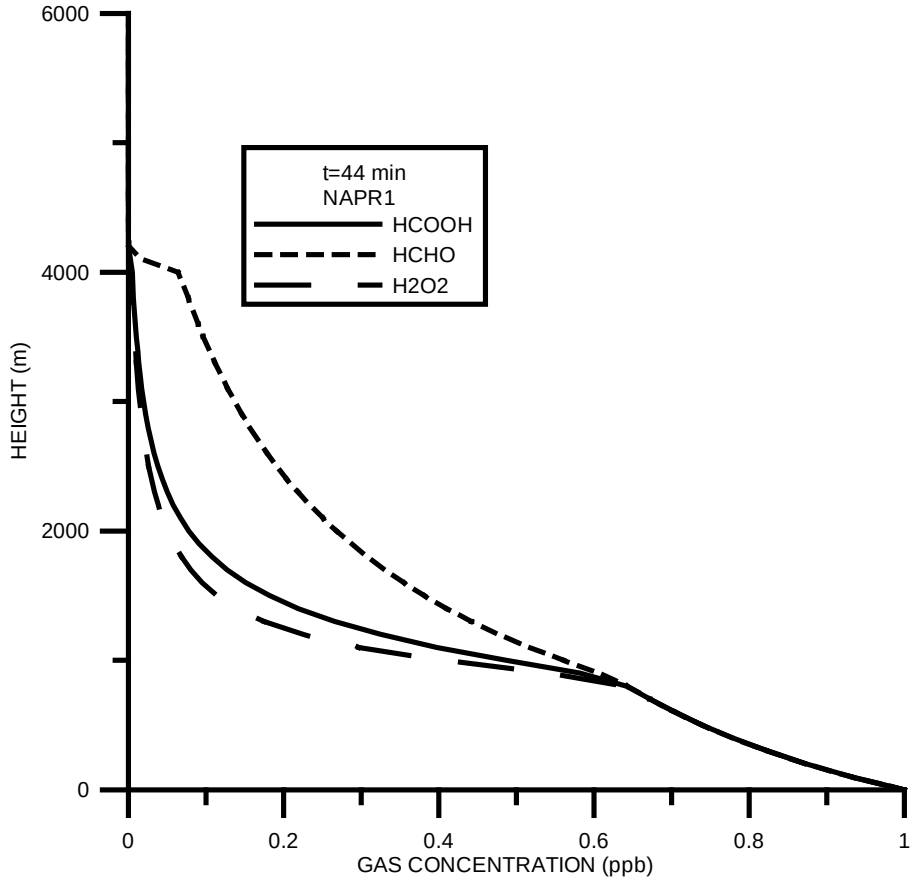

Fig. 2. Gas phase concentrations (ppb) of H_2O_2, HCHO and HCOOH as a function of height after 44 min of simulation, for the case with no aqueous phase oxidation.

ACPD
4, 591–634, 2004

Estimating the impact of natural and anthropogenic emissions

L. Alfonso and G. B. Raga

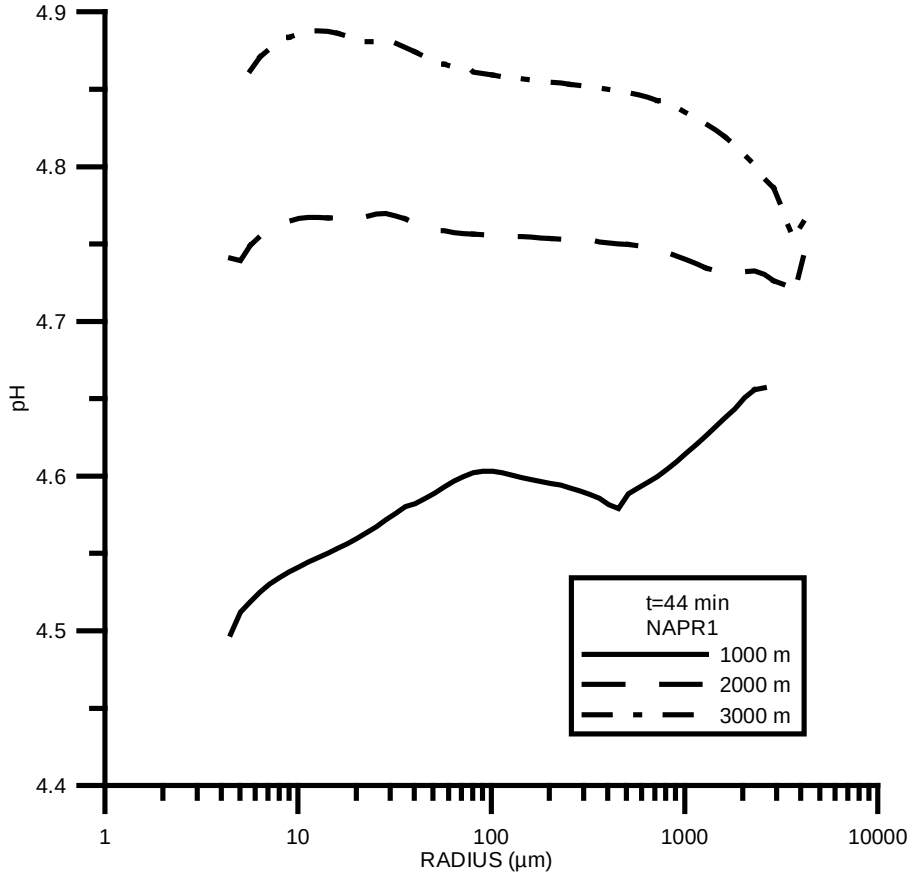

Fig. 3. pH at three different incloud levels after 44 min of simulation, for the case with no aqueous phase oxidation and an initial gas-phase concentration of formic acid of 1 pbb (NAPR1).

ACPD
4, 591–634, 2004

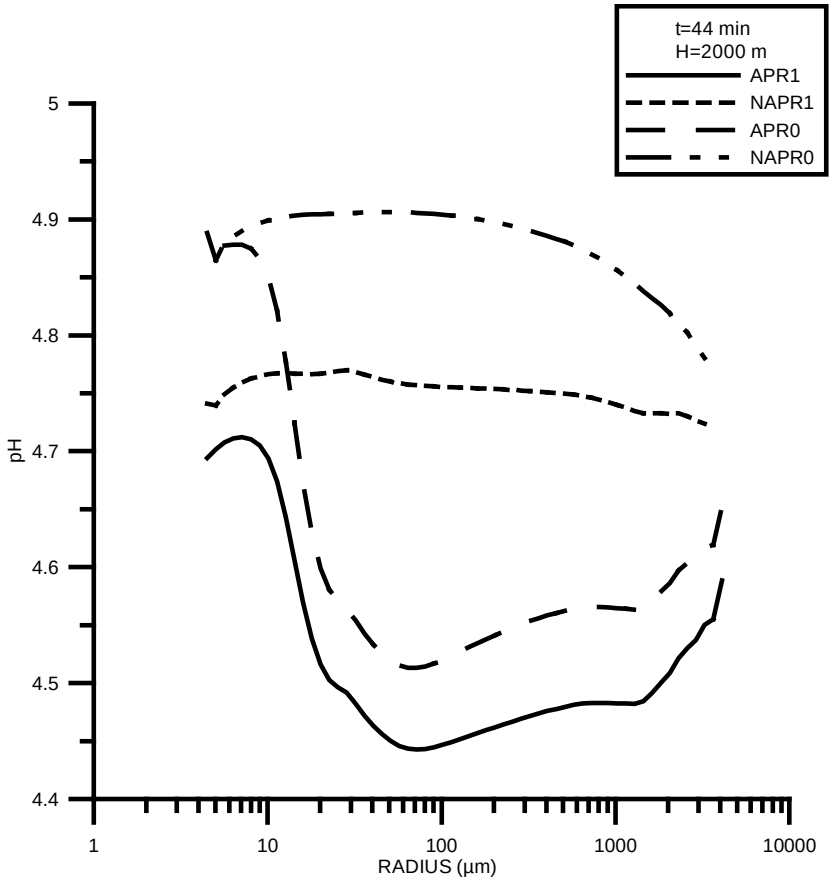

Fig. 4. pH at 2000 m for the cases with aqueous phase oxidation and an initial gas-phase concentration of formic acid of 0 and 1 ppb, respectively (APR0, APR1) and no aqueous-phase oxidation (NAPR0, NAPR1), after 44 min of simulation.

ACPD
4, 591–634, 2004

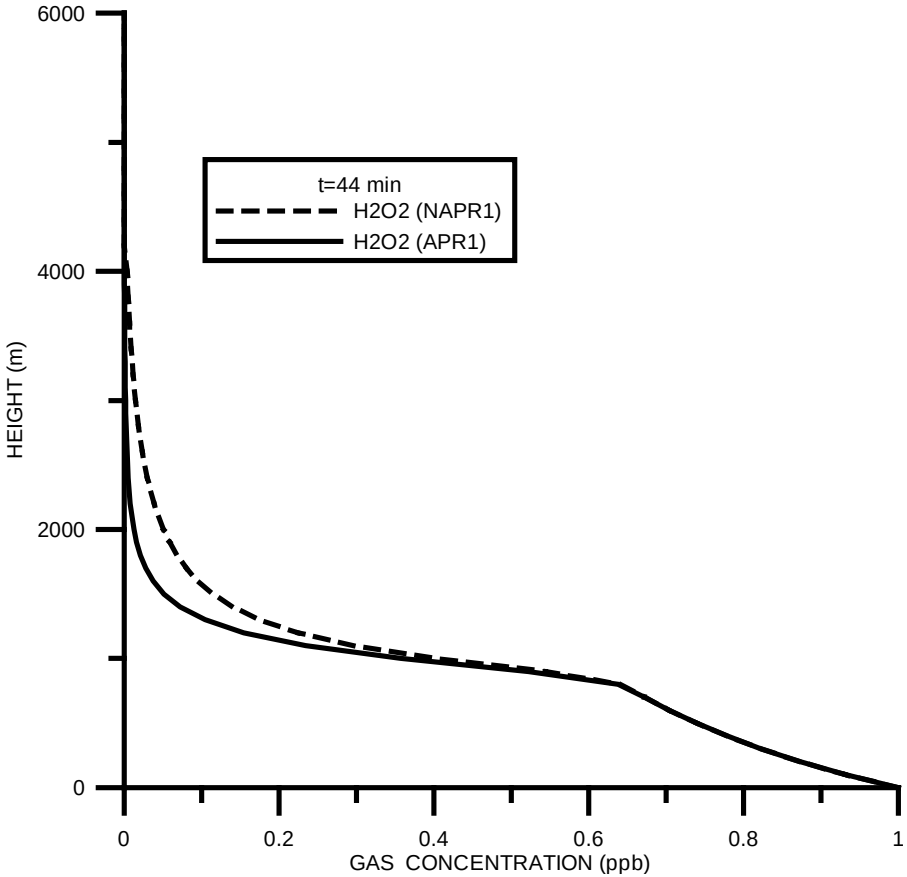

Fig. 5. Gas-phase H_2O_2 concentration (ppb) as a function of height for the cases with aqueous and no aqueous-phase oxidation, an initial formic acid gas-phase concentration of 1 ppb, and high (20 ppb) SO_2 ambient concentration (APR1, NAPR1), after 44 min of simulation.

ACPD
4, 591–634, 2004

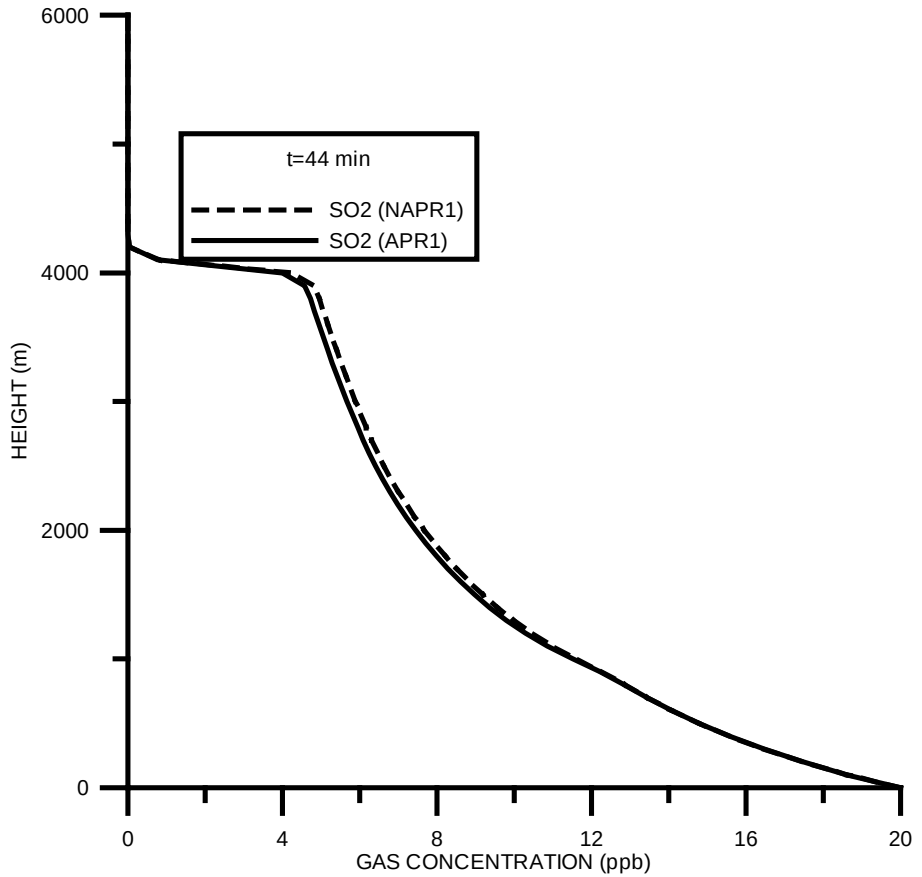

Fig. 6. Gas-phase SO_2 concentration (ppb) as a function of height for the cases with aqueous and no aqueous-phase oxidation, an initial formic acid gas-phase concentration of 1 ppb, and high (20 ppb) SO_2 ambient concentration (APR1, NAPR1), after 44 min of simulation.

ACPD
4, 591–634, 2004

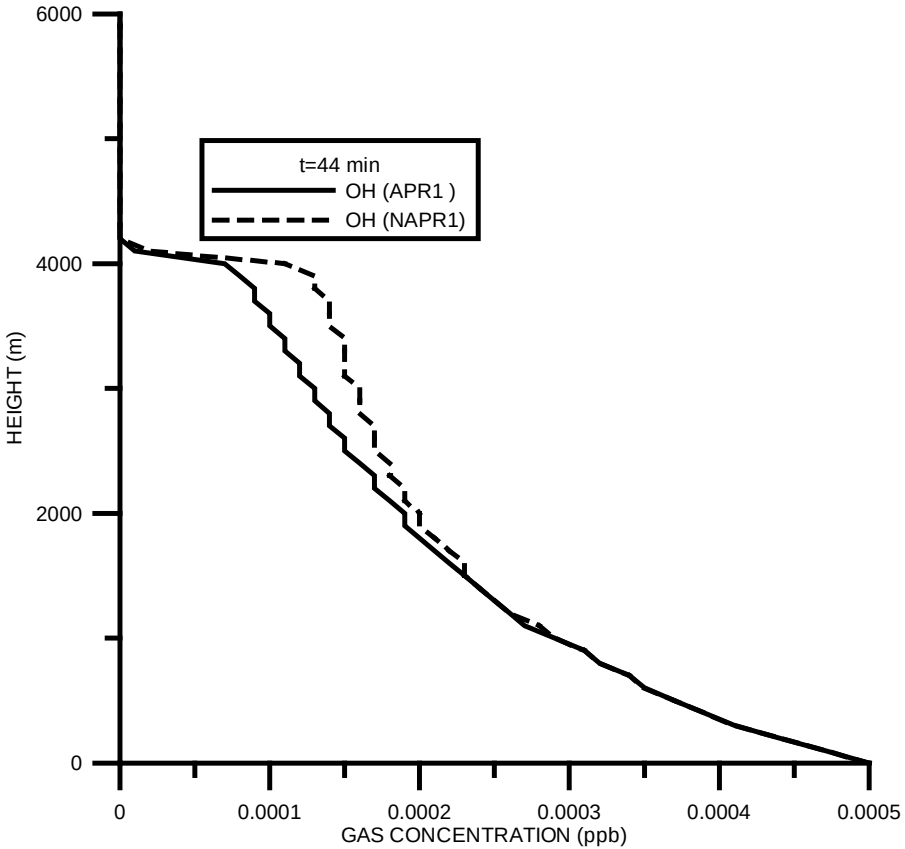

Fig. 7. Same as Fig. 6 but for OH concentration.

ACPD
4, 591–634, 2004

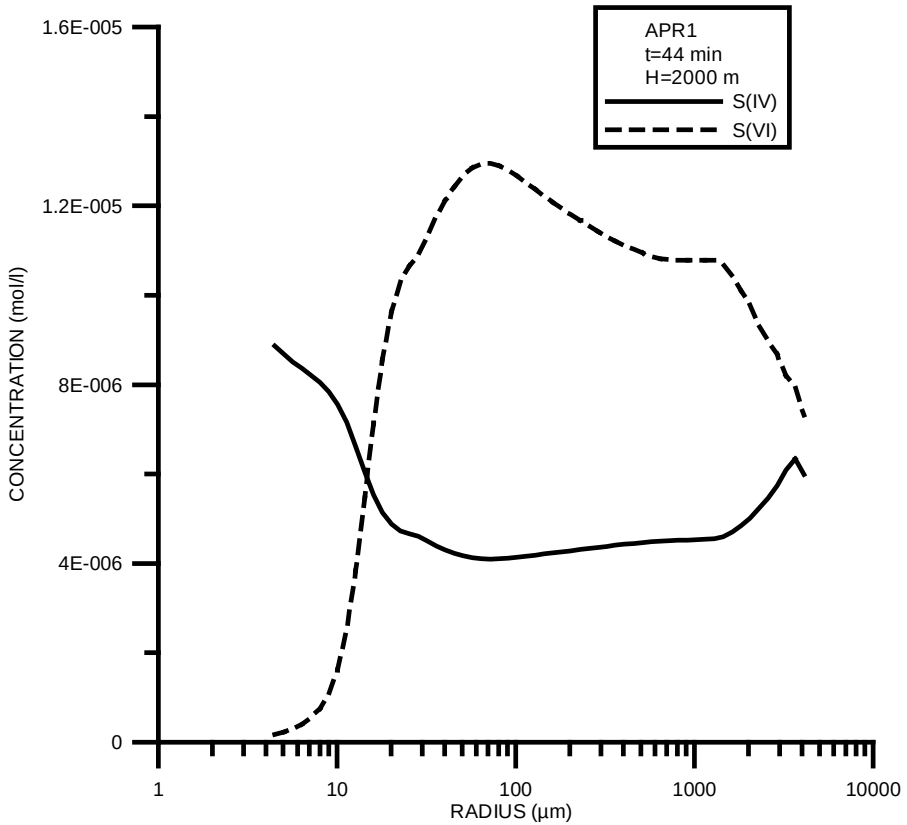

Fig. 8. S(IV) and S(VI) aqueous phase concentrations at 2000 m for the case with aqueous-phase oxidation, an initial formic acid gas-phase concentration of 1ppb and high (20 ppb) SO_2 ambient concentration (APR1), after 44 min of simulation.

ACPD
4, 591–634, 2004

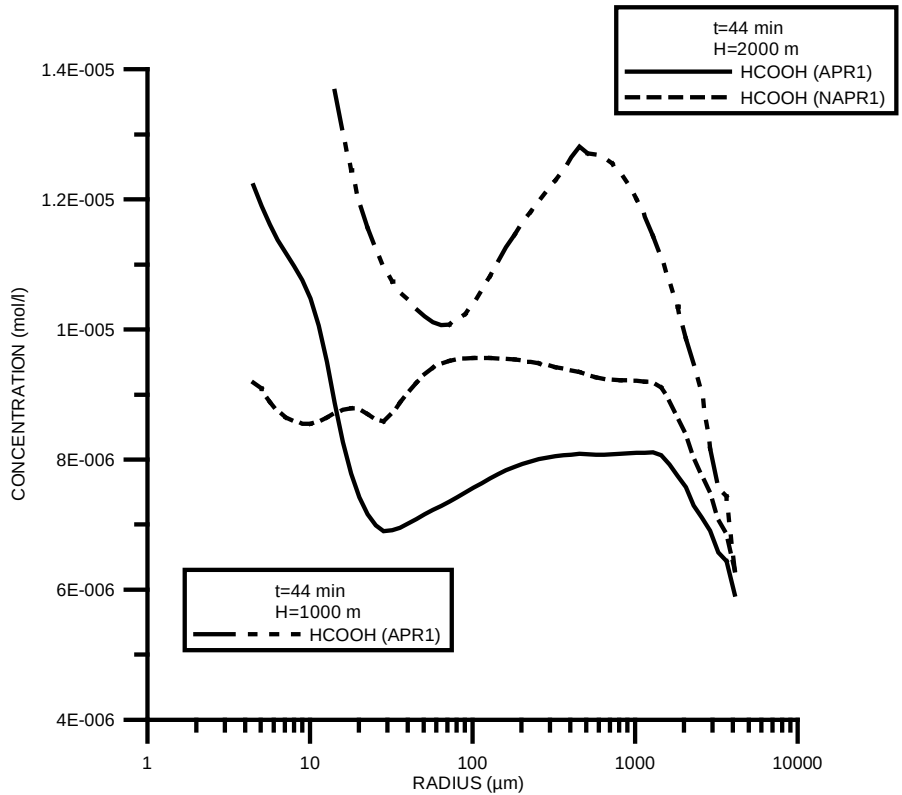

Fig. 9. HCOOH aqueous phase concentration at two different incloud levels (1000 and 2000 m), for the cases with aqueous phase oxidation, and no aqueous phase oxidation, an initial formic acid gas-phase concentration of 1 ppb and high (20 ppb) SO_2 ambient concentration (APR1, NAPR1), after 44 min of simulation.

ACPD
4, 591–634, 2004

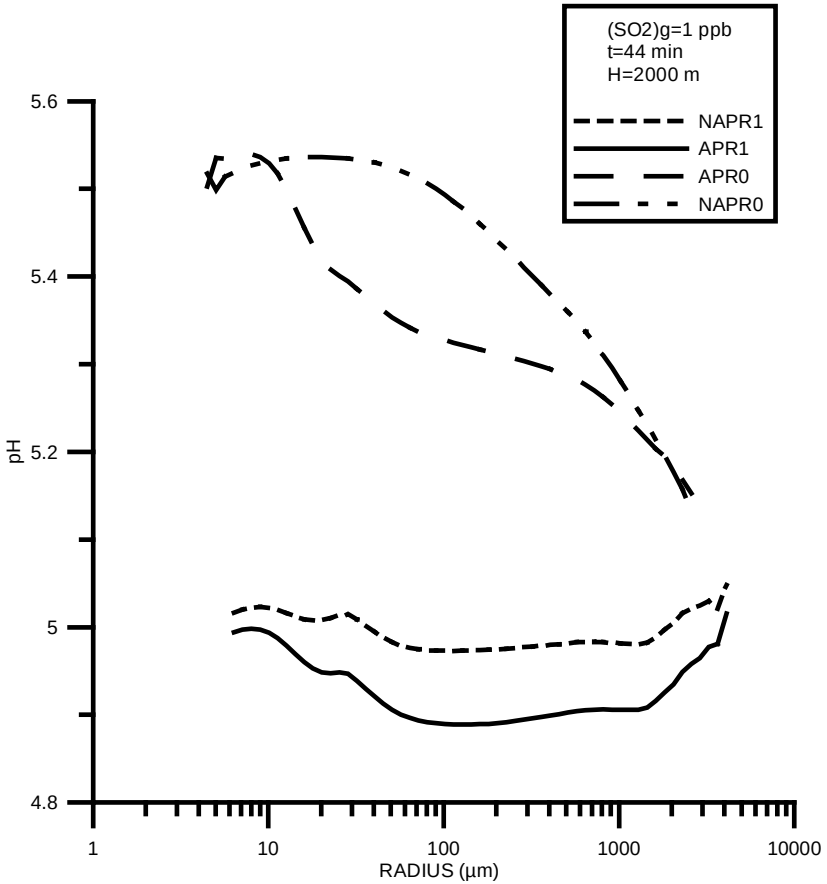

Fig. 10. pH at 2000 m for the cases with aqueous phase oxidation and an initial gas-phase concentration of formic acid of 0 and 1 ppb, respectively (APR0, APR1) and no aqueous-phase oxidation (NAPR0, NAPR1), and a low ambient SO_2 concentration (1 ppb), after 44 min of simulation.

ACPD
4, 591–634, 2004